Available online at www.sciencedirect.com
ScienceDirect
International Journal of Heat and Mass Transfer 51 (2008) 2060–2074
International Journal of HEAT and MASS TRANSFER
www.elsevier.com/locate/ijhmt

Thermal *in vivo* skin electroporation pore development and charged macromolecule transdermal delivery: A numerical study of the influence of chemically enhanced lower lipid phase transition temperatures

S.M. Becker, A.V. Kuznetsov *

Department of Mechanical and Aerospace Engineering, North Carolina State University, Campus Box 7910, Raleigh, NC 27695, United States

Received 22 December 2006; received in revised form 4 June 2007
Available online 30 July 2007

Abstract

Electroporation is an approach used to enhance transdermal transport of large molecules in which the skin is exposed to a series of electric pulses. Electroporation temporarily destabilizes the structure of the outer skin layer, the stratum corneum, by creating microscopic pores through which agents, which ordinarily are unable to pass into the skin, are able to pass through this outer barrier. Long duration electroporation pulses can cause localized temperature rises which result in thermotropic phase transitions within the lipid bilayer matrix of the stratum corneum. Chemical agents applied to the skin can reduce the lipid phase transition temperatures. This paper studies the benefits of the combination of the chemical enhancer, terpene d-limonene with low voltage electroporation pulses in order to further aid in electroporation pore development resulting from fluidization of the lipid structures within the stratum corneum. A transient finite volume model is developed in which the thermal and electrical behavior associated with electroporation of *in vivo* human skin is analyzed and lipid phase transition is represented by a melting process. The Nernst–Planck model is used to represent the electrophoretic-assisted transport of large charged molecules through the skin. The results show that the lower lipid phase transition temperatures associated with the topical application of chemical enhancers to the skin allow for increased solute delivery and solute penetration of the skin reaching radial locations much further than in the untreated case. Solute transport solutions of both cases exhibit local accumulation of concentrations below the stratum corneum – epidermis interface which exceed concentration values initially contained within the applicator gel.

1. Introduction

The thin (10–20 μm) outermost layer of the skin, the stratum corneum (SC), acts as a barrier inhibiting transdermal drug delivery. The SC is composed of flat dead cell shells, called corneocytes, which are interconnected by a lipid lamellar bilayer structure in a crystalline-gel phase. The barrier function of the SC is primarily associated with this lamellar lipid structure in the extracellular space of the SC [1,2]. Electroporation has been shown to greatly increase the success of transdermal delivery of large molecules [3–5]. During skin electroporation, the skin is exposed to a series of intense electric pulses in order to change the structure of the SC by creating microscopic aqueous pores [6–8]. The breakdown of the SC barrier function allows for increased molecular transport and radically reduces the electrical resistance of the skin [6,9–12]. Although the primary effects of electroporation are these microscopic transient pores, under certain pulse parameters, secondary effects occur resulting from Joule heating and the associated highly localized regions of elevated temperatures. At temperatures around 70 °C the SC lipid lamellar structure

* Corresponding author. Tel.: +1 919 515 5292; fax: +1 919 515 7968.
E-mail addresses: smbecker@unity.ncsu.edu (S.M. Becker), avkuznet@eos.ncsu.edu (A.V. Kuznetsov).

0017-9310/$ - see front matter © 2007 Elsevier Ltd. All rights reserved.
doi:10.1016/j.ijheatmasstransfer.2007.06.010

is compromised [13–17] and subsequently the barrier function of the SC is dramatically reduced [14,18]. It is recognized that localized Joule heating associated with electroporation is likely to contribute to increased permeability of the SC by lipid chain melting [4,19–22]. In [4,19] *in vitro* studies show that for moderate voltage, long duration pulses, electroporation pores originate within existing trans-SC appendageal pathways (sweat glands or hair follicles) and it is postulated that large current densities within the pore result in localized Joule heating and temperature rises sufficient to cause lipid phase transitions within the surrounding SC. Further *in vitro* experiments show that the effective pore radius of the localized transport region (LTR) is proportional to pulse duration which is associated with Joule heating [20]. Evidence of lipid phase change brought on by localized Joule heating is also presented in [21] where correlations between mass permeability of the SC and local temperature rise above lipid phase transition are established.

The skin barrier property has also been shown to be overcome by chemical penetration enhancers which act to destabilize the transport hindrance by interacting with the SC bilayer structure resulting in increased passive diffusion fluxes [23]. One class of chemical enhancers, terpenes, which are found in some plant oils, have been shown to decrease the temperatures at which SC lipids experience phase transition [16] and increase transdermal mass flux during iontophoresis (a very low voltage electro-assisted transport method) [24]. Chemical enhancers have been used in conjunction with electroporation experimentally in order to prolong the recovery of the electroporated SC bilayers [4].

Previous models of transdermal electrically assisted molecular transport focusing on iontophoresis are predominantly one-dimensional, and treat the skin as a homogeneous membrane [25–28]. By treating the SC as a homogeneous membrane any local variations of the electric field within the SC are neglected, and the radial gradients in mass flux cannot be represented. By modeling the skin as a single membrane, variations in axial concentration of solute deposition are lost. In [29] a theoretical model is developed in which a high voltage electroporation pulse about an existing small diameter pore causes temperature rises which are sufficient to thermally alter the SC's lipid structure.

The current study's purpose is first to develop a two-dimensional transient model of skin electroporation which captures thermal pore development and local solute transport. The model emphasizes the coupling of the thermal and electrical solutions with the SC lipid phase transition. As the lipid configuration changes from lamellar to disordered due to local temperature rises, the model incorporates dramatic drops in electrical and transport resistance. Then, using this model, the study shows that combining terpene enhancer with skin electroporation greatly increases the success of transdermal mass transport.

1.1. Physical model

This paper considers the effects of skin electroporation in the direct vicinity of an electroporation pore. Typically in external skin electroporation a section of skin coated with an applicator gel is pinched between two electrodes (see Fig. 1a). Computations preformed in this study rely on symmetry at the axial mid-plane ($z = W/2$), therefore only the half domain is modeled. In this study a small section of tissue near the center of the electrode is used to represent the target region. Fig. 1b shows the composite representation of this configuration consisting of electrodes (e), gel (g), and skin. The skin model consists of four sections: SC, epidermis (ED), dermis (DERM), and subcutaneous fat (FAT). This model uses a cylindrical domain with an outer radius $R_O = 1$ mm. Fig. 1c shows a representation of the SC prior to electroporation in which a pre-existing pore of radius $R_P = 5$ μm at the axial center passes through the SC. Prior to electroporation, the lipid structure connecting the corneocytes of the SC is the lamellar and uniform. During electroporation a large current density through the pore causes local temperature rises within the SC. Fig. 1d shows the lamellar structure in phase transition and that the effective pore radius, R_{eff}, extends to the region at which SC lipids are unaffected by the temperature rises. The axial axis origin begins at the SC–gel interface and is oriented positive into the skin, while the radial axis origin is at the center. Table 1 lists the composite thicknesses used in this model.

1.2. Mathematical model

1.2.1. Thermal energy

In formulating the thermal model, the system is divided into three sub-domains: composite tissue, applicator gel, and electrode plate.

To represent the composite tissue domain, the Pennes' bioheat equation [32] is used along with an additional source term:

$$\rho_i c_i \frac{\partial T}{\partial t} = \nabla \cdot (k_i \nabla T) - \omega_i c_b (T - T_a) + q_i''' + Q_J \tag{1}$$

where ρ is the density, c is the specific heat, k is the thermal conductivity, T is the temperature, T_a is the arterial temperature, Q_J is the Joule heat generated from the induced electric field, q''' is the metabolic volumetric heat generation, ω_m is the non-directional blood flow associated with perfusion, t is the time. The parameter c_b in the perfusion term is the specific heat of blood, which is assigned a value of $c_b = 3800$ J/kg K [33]. The subscript i refers to one of the four composite skin layers: SC, ED, DERM, or FAT.

The gel layer (g), situated between the electrode and the SC is represented by the transient conduction equation with an added source term representing Joule heating:

$$\rho_g c_g \frac{\partial T_g}{\partial t} = \nabla \cdot (k_g \nabla T_g) + Q_J \tag{2}$$

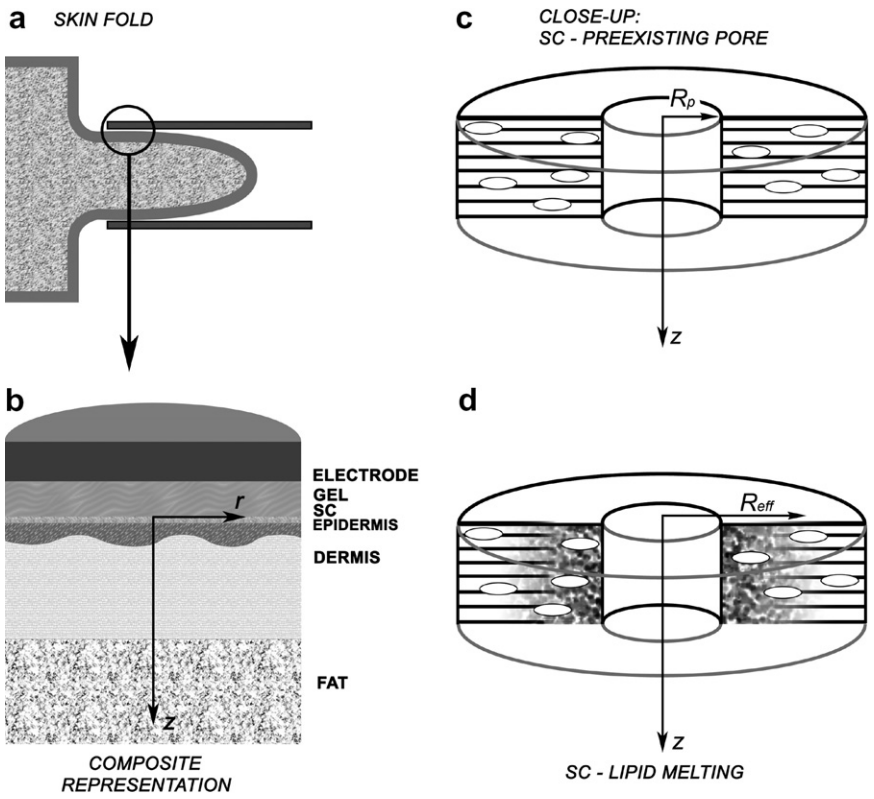

Fig. 1. Physical model description: (a) electroporation skin fold overview, (b) composite skin layers (cylindrical representation), (c) close-up of trans-SC pre-existing pore with unperturbed lipid configuration, (d) close-up of electroporated SC: lipids undergoing structural phase transition.

Table 1
Composite material dimensions and properties

	SC	ED	DERM	FAT	g	e
Thickness, δ (mm)	0.015 [30]	0.035 [30]	1.1 [31]	1.2 [31]	1	1
Thermal conductivity, k (W/m K)	0.2 [34]	0.209 [35]	0.293 [35]	0.23 [33]	0.6	16
Density, ρ (kg/m^3)	1500 [33]	1110 [33]	1116 [33]	850 [36]	1000	7850
Heat capacity (specific), c (J/kg K)	3600 [36]	3600 [36]	3800 [36]	2300 [36]	4180	450
Perfusion, ω (kg/m^3 s)	0	0	2.33 [37]	0.545 [37]	–	–
Metabolic heat generation, q''' (W/m^3)	0	0	200 [36]	5 [36]	–	–
Electrical conductivity, σ (S/m)	10^{-5} [33] ($\sigma_{SC,MELT} = 0.001$)	0.01	0.015	0.02 [33]	1.5	–
Electrophoretic mobility, m (m^2/V s)	10^{-17} ($m_{SC,MELT} = 5 \times 10^{-11}$)	10^{-10}	2×10^{-10}	10^{-10}	10^{-8}	–
Diffusivity, D (m^2/s)	10^{-17} ($D_{SC,MELT} = 10^{-13}$)	10^{-12}	10^{-12}	10^{-12}	10^{-9}	–

This domain also includes the pre-existing trans-SC pore which is contained in the central 5 μm radius section of the SC.

The electrode plate section (e) is represented by the transient conduction equation:

$$\rho_e c_e \frac{\partial T_e}{\partial t} = \nabla \cdot (k_e \nabla T_e) \tag{3}$$

where the subscript e refers to electrode plate parameters. Tissue, electrode and gel property values used are listed in Table 1.

1.3. Boundary and initial conditions

Initially the temperatures of the composite tissue, and gel domains are assumed to be equal to the arterial blood temperature, T_a:

$$T_i(r,z,0) = T_a \tag{4}$$

$$T_g(r,z,0) = T_a \tag{5}$$

The electrodes are added to the model at the onset of the first electroporation pulse, and unless otherwise specified are left in contact with the target region for all remaining computations. Initially electrodes are assumed to have the same temperature as the surroundings, T_∞:

$$T_e(r,z,0) = T_\infty \tag{6}$$

The outer radial faces of the tissue, gel and electrode domains are assumed thermally insulated:

$$\frac{\partial}{\partial r} T(R_0,z,t) = 0 \tag{7}$$

A convective flux boundary condition is imposed onto the electrode face exposed to the ambient air:

Table 2
Operational parameter values

Computational domain radius	R_0	1 mm
Pre-existing pore radius	R_P	5 μm
Arterial blood temperature	T_a	37 °C
Ambient temperature	T_∞	20 °C
Convection coefficient	h	15 W/m^2 K
Applied voltage	V_{app}	275 V
Pulse duration	τ_P	200 ms
Pulse interval	τ_S	1 s
Number of pulses delivered	N_P	4

$$q'' = h(T_e - T_\infty) = -k_e \left.\frac{\partial T_e}{\partial z}\right|_{surface} \tag{8}$$

where q'' is the heat flux convected from the exposed face, h is the convection coefficient, and T_∞ is the ambient air temperature.

Symmetry is applied at the skin fold axial midpoint:

$$\frac{\partial}{\partial z} T_{FAT}(r, W/2, t) = 0 \tag{9}$$

where W is the plate spacing. Table 2 lists further parameter values.

1.4. Electric field power generation

During electroporation the induced electric field causes a temperature rise due to Joule heating. The power supplied is found as follows. The electric potential is solved from the Laplace equation:

$$\nabla \cdot (\sigma_i \nabla \phi) = 0 \tag{10}$$

where ϕ is the electric potential and σ_i is the composite electrical conductivity, and the subscript i refers to one of the composite layers: g, SC, ED, DERM, or FAT. This equation is solved using the boundary condition at the upper electrode–gel interface, in which the potential is the same as the applied voltage, V_{app}:

$$\phi(r, -\delta_g) = V_{app} \tag{11}$$

where δ_g is the thickness of the gel section. The second boundary condition uses symmetry of the system imposing a potential value equal to half of the applied voltage at the target region axial middle:

$$\phi(r, W/2) = V_{app}/2 \tag{12}$$

where W is the spacing between electrodes.

In this study a direct current pulse is modeled with an applied voltage value of $V_{app} = 275$ V.

The outer radial surface of the target region is assumed electrically insulated:

$$\frac{\partial}{\partial r} \phi(R_0, z) = 0 \tag{13}$$

The power due to Joule heating is then defined as

$$Q_J = \sigma_i |\nabla \phi|^2 \tag{14}$$

Obviously there is no Joule heating outside the target region or at times during which the electric pulses are not applied. In [38] it is shown that even at moderate voltages the capacitive charging time associated with non-Ohmic behavior of the skin is very short and may be neglected at times greater than 1 ms. This behavior is neglected in this study. Eq. (10) neglects the influence of the charged molecules of the solute on the electrical distribution of the large magnitude pulse.

1.5. Mass transport

Electrically driven transdermal delivery is negotiated by the three modes of transport: electrophoresis, electro-osmosis, and diffusion. Studies focusing on electrically driven transport of large charged molecules show that electro-osmotic effects are negligible compared to electrophoresis forces [39] (especially for short duration pulses). Homogenous tissue *in vivo* electroporation studies show that electrophoretic forces dominate in the transport of large molecules [40,41]. In skin electroporation the pulse parameters are short (compared to iontophoresis), thus electro-osmosis plays a negligible role, while electrophoresis effects are the primary effects in transdermal delivery of charged molecules [4,5].

The transport of solute through the SC and into the underlying domain is formulated from the Nernst–Planck equation [42] as follows:

$$\frac{\partial C}{\partial t} = -\nabla \cdot (m_i C \nabla \phi) - \nabla \cdot (D_i \nabla C) \tag{15}$$

where D is the diffusion coefficient, m is the electromobility, and the subscript i refers to one of the composite layers: g, SC, ED, DERM, or FAT, and C is the local dimensionless solute concentration, which is defined by the relation:

$$C = \frac{C^*}{C_0} \tag{16}$$

where C^* is the local solute concentration and C_0 is the initial concentration within the gel layer.

Eq. (15) is solved using the zero flux conditions:

$$\left.\frac{\partial C}{\partial r}\right|_{r=R_0} = \left.\frac{\partial C}{\partial r}\right|_{r=0} = \left.\frac{\partial C}{\partial z}\right|_{z=-\delta_g} = 0 \tag{17}$$

The last boundary condition used is justified by the assumption that, given the short time periods of evaluation and small magnitude transport parameter values, the solute is not expected to be transported to the lower computational boundary:

$$C(r, W/2, t) = 0 \tag{18}$$

Initially all the solute is contained within the gel layer:

$$C(r, z, 0) = \begin{cases} 1, & z < 0 \\ 0, & z > 0 \end{cases} \tag{19}$$

Exact correlations between electromobility and molecular weight and charge are not available although *in vitro* exper-

Table 3
SC lipid enthalpic phase transition data reflecting findings of [16]

Phase change	Association	Without enhancer $[T_1, T_2]$ (°C)	Terpene d-limonene $[T_1, T_2]$ (°C)	Without enhancer ΔH (J/kg)	Terpene d-limonene ΔH (J/kg)
E	Fluidization of lamellar lipids	[65, 75]	[45, 55]	5500	6000
F	Fluidization of protein associated lipids	[75, 90]	[55, 70]	4000	3900
G	Denaturation of proteins	[90, 110]	[70,110]	4700	3100

imental measurements of DNA movement in tumor tissues show that electrophoresis increases transport over passive diffusion by several orders of magnitude, and that transport increases with pulse intensity [39]. *In vitro* studies also show that collagen content and structure acts to reduce electromobility of large molecules in tumor tissue [39,43]. Electrophoresis studies in polyacrylamide and agarose gels have been conducted to estimate mobility of DNA within the interstitial spaces of living tissue [44,45]. These studies show that mobility varies inversely with gel concentration in the order of magnitude range 10^{-8}–10^{-9} m^2/V s. Diffusion coefficients of DNA have been obtained experimentally in agarose gels and result in a range of values 10^{-12}–10^{-14} m^2/s depending on gel concentration [44]. Diffusion coefficients and electromobility values used in the current study have been chosen with the findings in mind and are given in Table 1.

1.6. Lipid phase change

The lipid structure is known to become destabilized at elevated temperatures. It is generally accepted that there exist four main endothermic transitions in the SC in the temperature range 40–130 °C which have been independently confirmed by differential scanning calorimetry [13–17], although evidence exists of additional thermal transitions [46,47]. This paper focuses on three high temperature transitions of the SC, adopting the convention used in [46,47], phase changes E, F, and G. The enthalpic peaks of phase change G occur at temperatures above 90 °C and have been associated with protein denaturation [15,16,46]. Secondary lipid melting has been associated with phase change F at higher temperatures around 80 °C and has been linked to lipid covalently bonded to corneocytes [15,16]. Of great interest in this paper is phase change E which has primarily been attributed to the disordering of the lamellar lipid phase [16] and has been documented in numerous differential scanning calorimetry studies at endothermic peak temperatures from 65 to 72 °C [47]. Using X-ray diffraction microscopy it has been shown that the lipid lamellar structure in the SC is evident up to temperatures about 60 °C and then disappears within 10 °C [2,48]. Polarized light thermal microscopy of lipids extracted from the SC directly shows an overall fluidization of lipid structures at 60 °C [46]. Further evidence of lipid chain melting and increased permeabilization at this phase change is given in [14,18] where it is shown that the SC becomes more permeable to water flux abruptly at 70 °C. Table 3 lists the temperature ranges over which each of the three phase transitions are represented.

Skin penetration enhancers have been shown to increase the permeability of the SC by increasing the diffusivity, probably by disrupting the lipid bilayer of the SC [23]. In [16] the terpene d-limonene is shown to reduce both E and F phase transition temperatures by 20 °C. Enthalpic curves generated by differential scanning calorimetry also show that using this enhancer broadens the endotherm associated with phase change G. These findings are reflected in the enthalpy and phase change temperatures used in this study and provided in Table 3.

To capture SC lipid phase transition this study borrows from enthalpy methods which were originally designed to model melting and solidification processes occurring over a temperature range [49,50]. A rectangular shaped specific heat vs. temperature curve is used to model phase transitions as in [51,52]. The heat of transition is modeled using apparent specific heats as follows:

$$c_{\mathrm{SC,APP}} = c_{\mathrm{SC}} + c_{\mathrm{SC,L}} \tag{20}$$

where $c_{\mathrm{SC,APP}}$ is the apparent SC specific heat, and $c_{\mathrm{SC,L}}$ is the latent specific heat which is represented as

$$c_{\mathrm{SC,L}} = \frac{\Delta H_{\mathrm{PC}}}{T_{\mathrm{PC2}} - T_{\mathrm{PC1}}} \tag{21}$$

where ΔH is the latent heat, T_2 and T_1 are the representative phase change end and beginning temperatures, and the subscript PC refers to one of the three phase transitions: E, F, or G. Table 3 lists the values used in computations for the three SC phase change regions.

In light of the previously discussed SC lipid thermal behavior and permeability studied, this model uses phase transition E to model SC lipid melting during which the fraction of lipid melting is defined as

$$\varphi = \frac{(H - c_{\mathrm{SC}}T)}{\Delta H_{\mathrm{E}}} \tag{22}$$

where H is the total enthalpy and is defined:

$$H = \int_{T_{\mathrm{E1}}}^{T_{\mathrm{E2}}} c_{\mathrm{SC,APP}}\,\mathrm{d}T \tag{23}$$

Given the assumed linear endothermic absorption over the lipid melting region E, the fraction of lipid melt is represented as

$$\varphi = \begin{cases} 0, & T < T_{1,E} \\ \frac{T-T_{E,1}}{T_{E,2}-T_{E,1}}, & T_{E,1} < T < T_{E,2} \\ 1, & T_{E,2} < T \end{cases} \quad (24)$$

The electrical conductivity of the SC is several orders of magnitude lower than the underlying composite layers. The lamellar structure of the bilayer matrix greatly reduces ionic permeability. With the fluidization the lamellar lipid extracellular sheets in phase transition E comes increased SC ionic permeability. Electrical resistance has been shown to drop by two orders of magnitude in the temperature range of this phase change [53] which also suggests the barrier function of the SC is compromised in transition E.

To model the increase in electrical conductivity with lipid restructuring, the local SC effective electrical conductivity is related to lipid melt fraction by the relations:

$$\sigma^*_{SC} = \sigma_{SC} + \varphi(\sigma_{SC,MELT} - \sigma_{SC}) \quad (25)$$

where σ_{SC} is the normal electrical conductivity, and $\sigma_{SC,MELT}$ is the electrical conductivity associated with the SC after full lipid melting. To represent the two order of magnitude increase in electrical conductivity with lipid restructuring as suggested by the results of [53], in this study a value of $\sigma_{SC,MELT} = 0.001$ S/m is used.

Similarly enhanced electrokinetic mobility and diffusion coefficient of the SC are related to lipid melt fraction by the relations:

$$m^*_{SC} = m_{SC} + \varphi(m_{SC,MELT} - m_{SC}) \quad (26)$$

where m_{SC} is the unperturbed mobility of the SC, $m_{SC,MELT}$ is the mobility associated with the SC after full lipid melting; in this study a value of $m_{SC,MELT} = 5 \times 10^{-11}$ m^2/V s is used.

$$D^*_{SC} = D_{SC} + \varphi(D_{SC,MELT} - D_{SC}) \quad (27)$$

where D_{SC} corresponds to the initial diffusion coefficient of the solute in the SC, $D_{SC,MELT}$ is the diffusion coefficient associated with the SC after full lipid melting; in this study a value of $D_{SC,MELT} = 10^{-13}$ m^2/V s is used. The values used to represent the mass transport coefficients associated with the fully thermally altered SC have been chosen to approximate the very resistive conditions a large DNA molecule would experience within the tortuous route between the unaltered corneocytes of the SC: the approximated diffusion and electrophoretic mobility coefficients

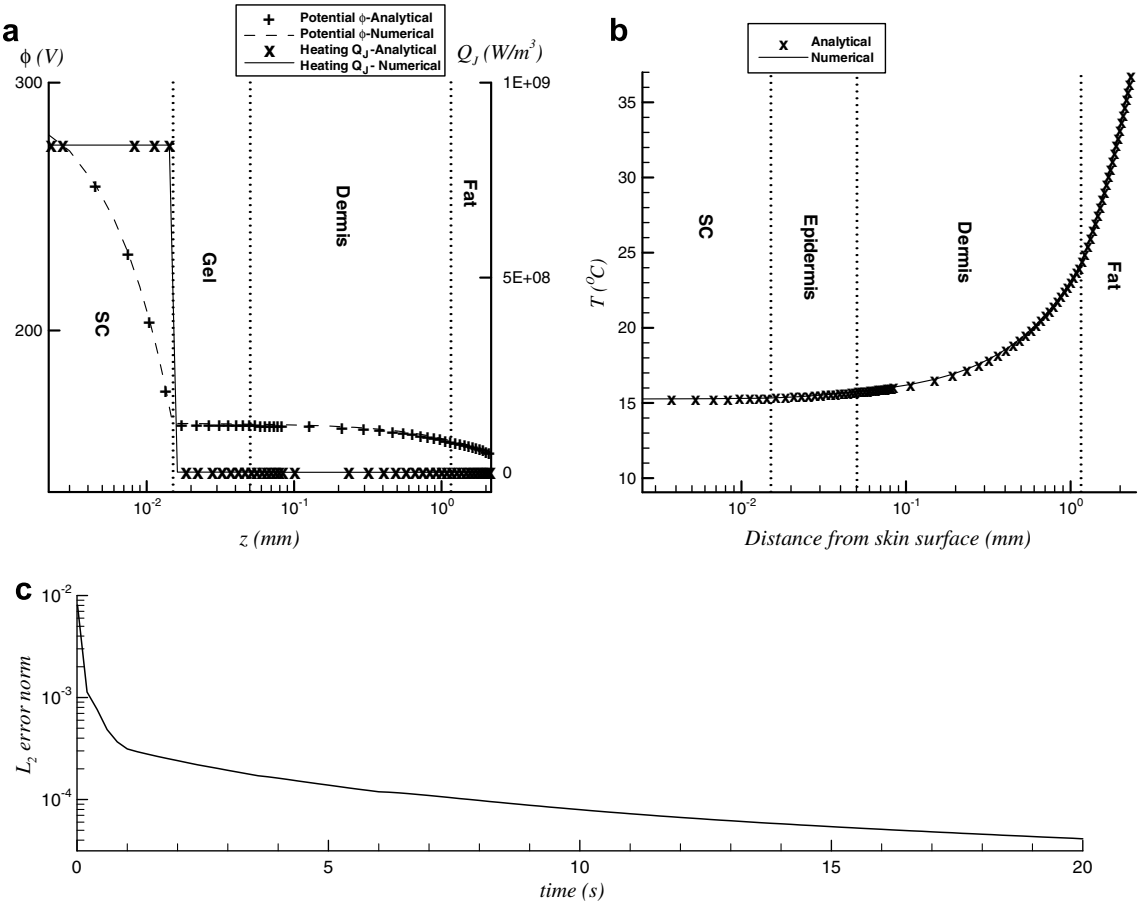

Fig. 2. Comparisons between numerical code and analytic solution (one-dimensional): (a) Electric (potential and heating) in which the domain represents a vertical line between the electrodes using $V_{app} = 300$ V. (b) Steady state temperature (°C), in which the domain represents vertical depth below the skin's surface using convection coefficient $h = 500$ W/m^3. Dotted lines separate composite sections. (c) L_2 normalized error of homogeneous two-dimensional solution comparison with analytical solution.

used are much lower than those associated with those of even the high collagen content tissue of the epidermis.

In [21,54] it is noted that long pulse duration is linked to increased post-pulse electrical resistance recovery times (>5 min). In [55] the electric and mass transport barrier properties of SC regions experiencing lipid thermal phase transition by electroporation show very long recovery times (>30 min). SC lipid structural changes associated with localized Joule heating during electroporation remain for some time after cooling of the SC [21]. Polarized light thermal microscopy of SC and extracted lipid samples heated to 130 °C show that as the SC samples return to room temperature, the restructuring of the lipids shows evidence of aggregate variation [46]. Because of these findings and in light of the relatively short time periods that transience is modeled (4s), upon cooling this study does not consider lamellar restructuring of the lipid bilayers and subsequent electrical recovery. Thus Eq. (24) is evaluated as

$$\varphi^{t+1} = \begin{cases} \max(\varphi^t, 0), & T < T_{1,E} \\ \max\left(\varphi^t, \frac{T - T_{E,1}}{T_{E,2} - T_{E,1}}\right), & T_{E,1} < T < T_{E,2} \\ 1, & T_{E,2} < T \end{cases} \tag{28}$$

where the superscript t and $t+1$ refers to the previous and current time steps, respectively.

2. Discretization and solution procedure

The computational domain is discretized using a variable cylindrical grid consisting of 34,100 cells. A fully implicit finite volume approach is used to solve Eqs. (1)–(3), (10) and (15). Temperature, T, and Joule heat, Q_J, are evaluated at the cell centers while the electric potential,

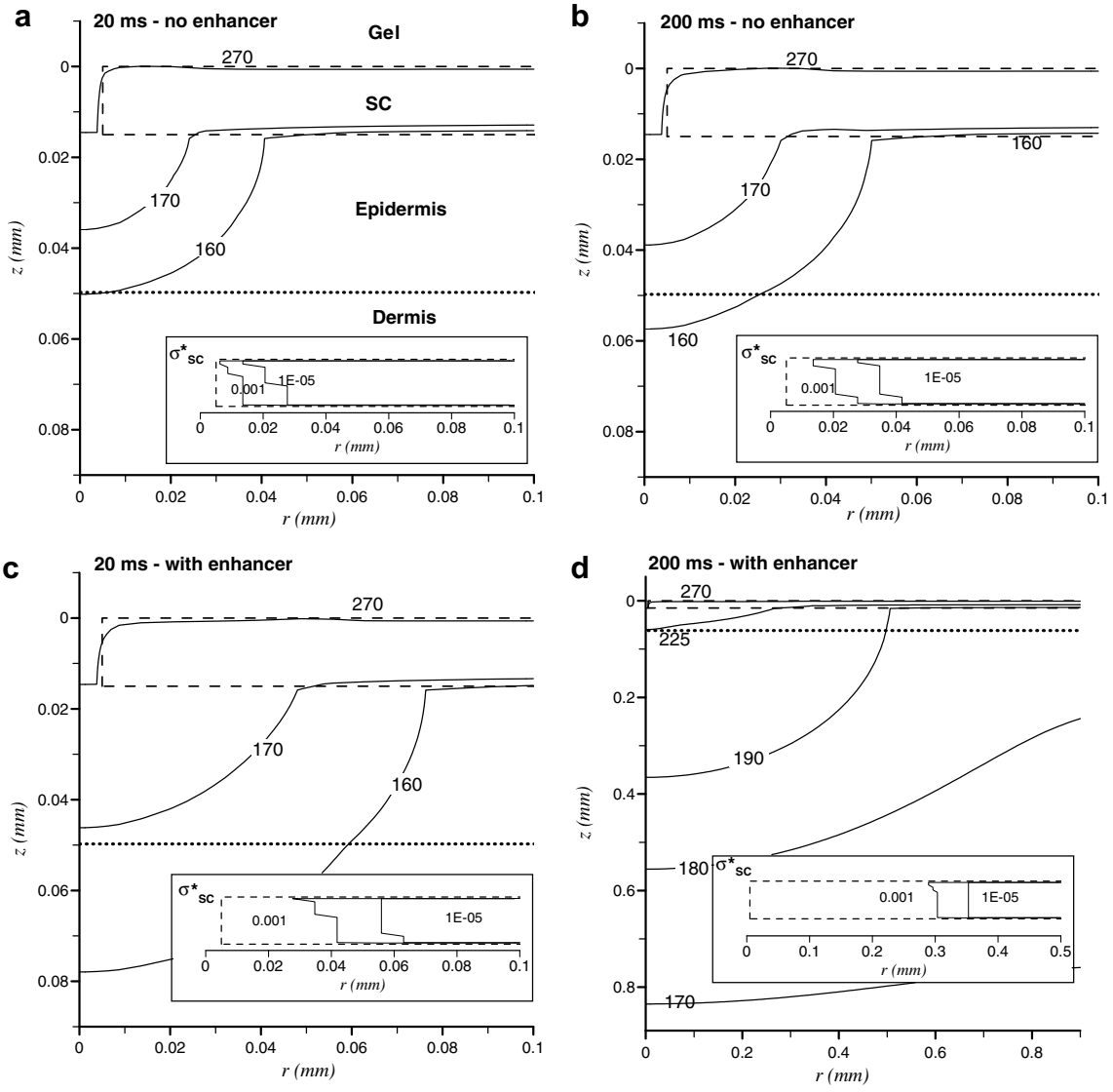

Fig. 3. Potential solution at representative pulsing times of a single 275 V pulse for cases without enhancer (a, b) and cases with enhancers (c, d). Dotted lines represent interfaces between composite layers. Dashed rectangle shows the boundary of the SC. Insets represent a close-up of the SC with contours denoting apparent electrical conductivity (S/m).

ϕ, is evaluated at the cell edges. The driving potential gradient, $\nabla\phi$, of the electrophoretic term in Eq. (15) is evaluated at the midpoint of the cell faces. A global 1 ms time step is used for transient Eqs. (1)–(3) and (15). Interface conductivity is represented by a harmonic mean similar to that described in [56], while a resistor representation is

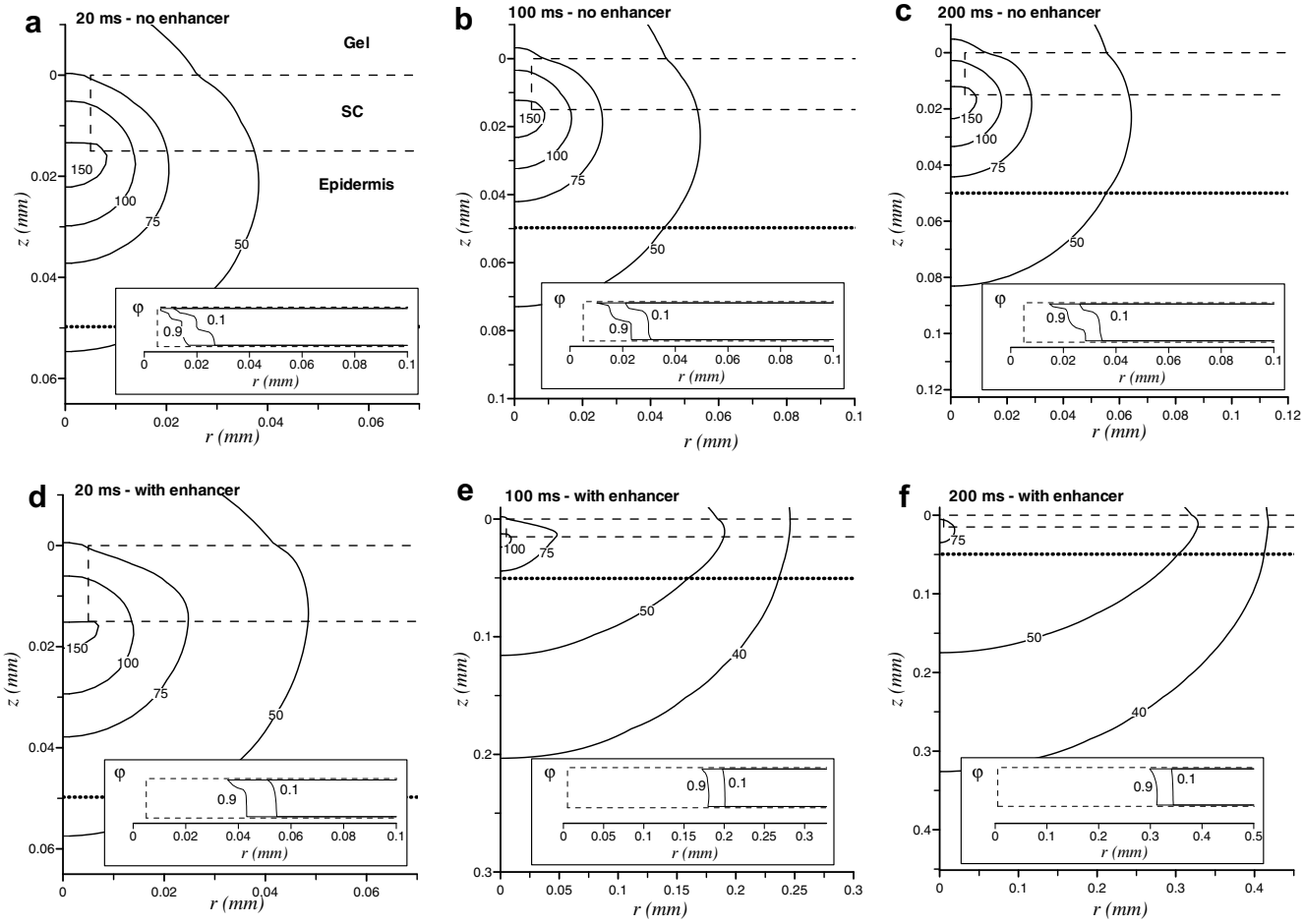

Fig. 4. Transient thermal solution (°C) at representative pulsing times of a single 275 V pulse for cases: without enhancer (a–c) and cases with enhancers (d–f). Dotted lines represent interfaces between composite layers. Dashed rectangle shows the boundary of the SC. Insets show lipid melt fraction contours in a close-up of the SC (dashed rectangle); inset (e) uses aspect ratio $x{:}y = 0.3{:}1$, inset (f) uses aspect ratio $x{:}y = 1{:}5$.

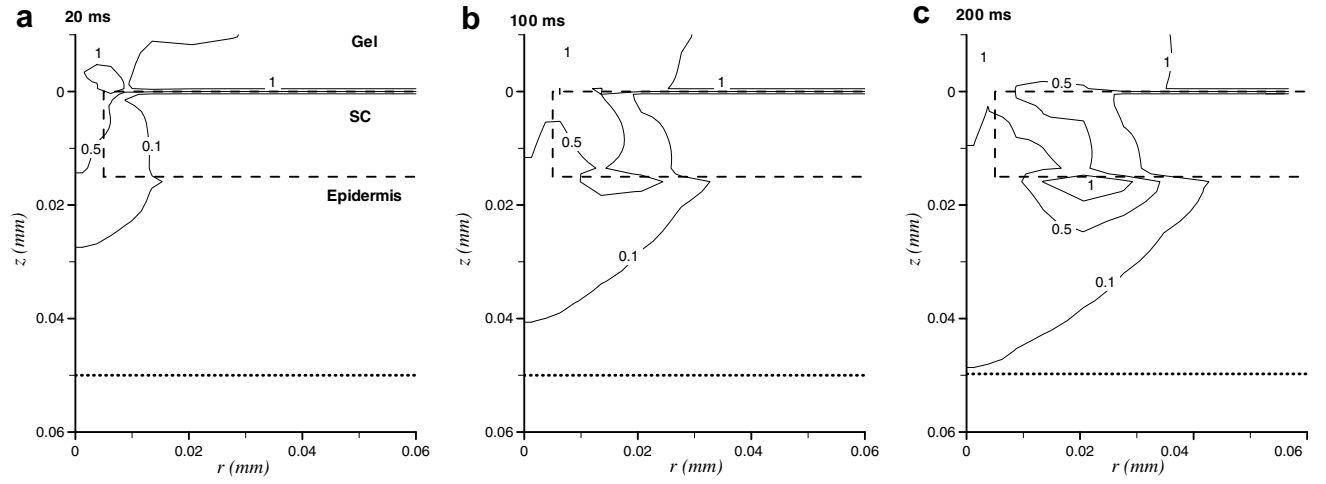

Fig. 5. Transient dimensionless concentration solution, C, of skin without enhancer treatment at representative pulsing times during a single 275 V pulse. Dashed rectangle shows the boundary of the SC. Dotted lines represent interfaces between composite layers.

used between the cell center and the convection boundary condition (8). The SC specific heats, mobility, diffusion coefficient, electrical conductivity and lipid melt fractions of Eqs. (25)–(28) are updated at each time step using the local temperature solution of the previous time step. Variables T, ϕ, and C are solved using an implicit point iterative method. Since it is expected that between time steps dramatic solution changes occur not over the entire solution domain, but locally within and about the target region (and within the effective pore radius), a localized convergence measure is used between iterations. The convergence criterion is defined as $\varepsilon = \left|T_{i,j}^{p+1} - T_{i,j}^{p}\right|$ where p is iteration and convergence is established when $\varepsilon < 10^{-5}$.

3. Code validation

To validate the numerical solution, comparisons with analytic solutions were made. The temperature solution of the one-dimensional steady form of Eq. (1) was obtained in the axial z-direction using parameter values: $h = 500$ W/m^2 K and $T_\infty = 10$ °C, and setting a prescribed temperature at the target region half width $T(W/2) = T_a$. The one-dimensional solutions of the electric potential and Joule heat Eqs. (10) and (14) are obtained along the axial direction. A SC conductivity value of $\sigma_{SC} = 10^{-5}$ S/m is used and the remaining composite tissue conductivity values are the same as in Table 1. Fig. 2a and b shows

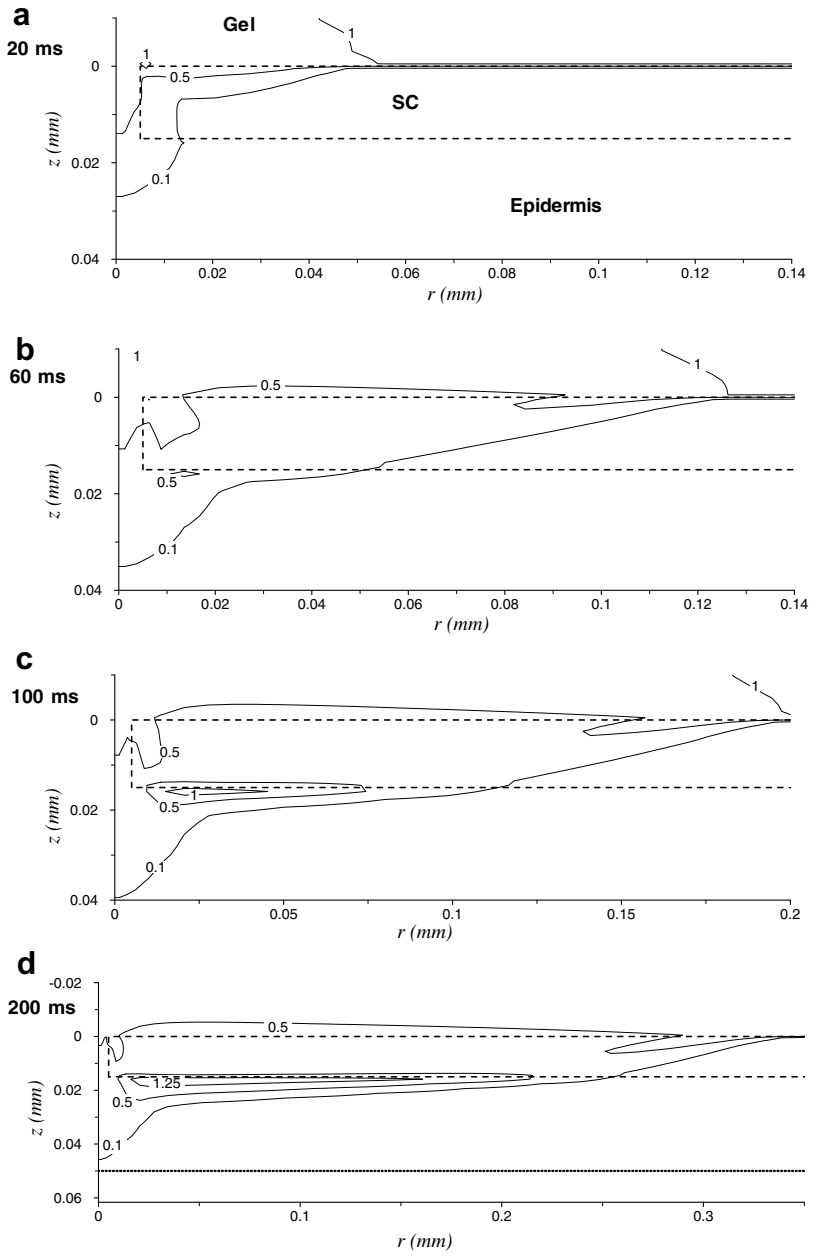

Fig. 6. Transient dimensionless concentration solution, C, of skin with enhancer treatment at representative pulsing times during a single 275 V pulse. Dashed rectangle shows the boundary of the SC. Dotted lines represent interfaces between composite layers.

excellent agreement between computed and analytic solutions. Eq. (15) is solved in a homogenous domain of diffusivity $D = 10^{-8}\,\mathrm{m^2/s}$ with zero applied potential and boundary conditions:

$$\left.\frac{\partial C}{\partial r}\right|_{r=0} = \left.\frac{\partial C}{\partial z}\right|_{z=W/2} = 0 \tag{29}$$

$$C|_{r=R_0} = C|_{z=0} = 1 \tag{30}$$

The solution results are compared to the analytic solution in Fig. 2c which shows the L_2 root mean square error norm. Again excellent agreement between numerical code and the analytic solution is established.

4. Results and discussion

Solute concentration, electric potential, and thermal solutions of interest are highly localized within and about the SC, and therefore solutions are presented at locations near the SC and not over the entire computational domain.

4.1. Single pulse

In order to show the phenomenon associated with the thermal, electrical, and transport solutions during pore formation, comparisons between cases with the enhancer and without the enhancer are presented during a single 200 ms pulse with an applied voltage of 275 V. Pulsation influences will be presented in later sections. The potential solution in the half domain at the beginning and end of the pulse is shown for skin without enhancement (Fig. 3a and b) and skin treated with the enhancer (Fig. 3c and d). The local apparent SC electrical conductivity is shown in the small inserts in which the two σ^*_{SC} contours shown represent the electrical conductivity associated with lipid structures thermally unaltered (10^{-5} S/m) and the conductivity of lipid structures that have become completely fluidized (0.001 S/m). Early in pulse application, at $t = 20$ ms (Fig. 3a and c), nearly the entire potential drop of the domain occurs across the SC. Even at this early time, the case with the enhancer shows evidence of increased pore development in the slightly more spread potential drops

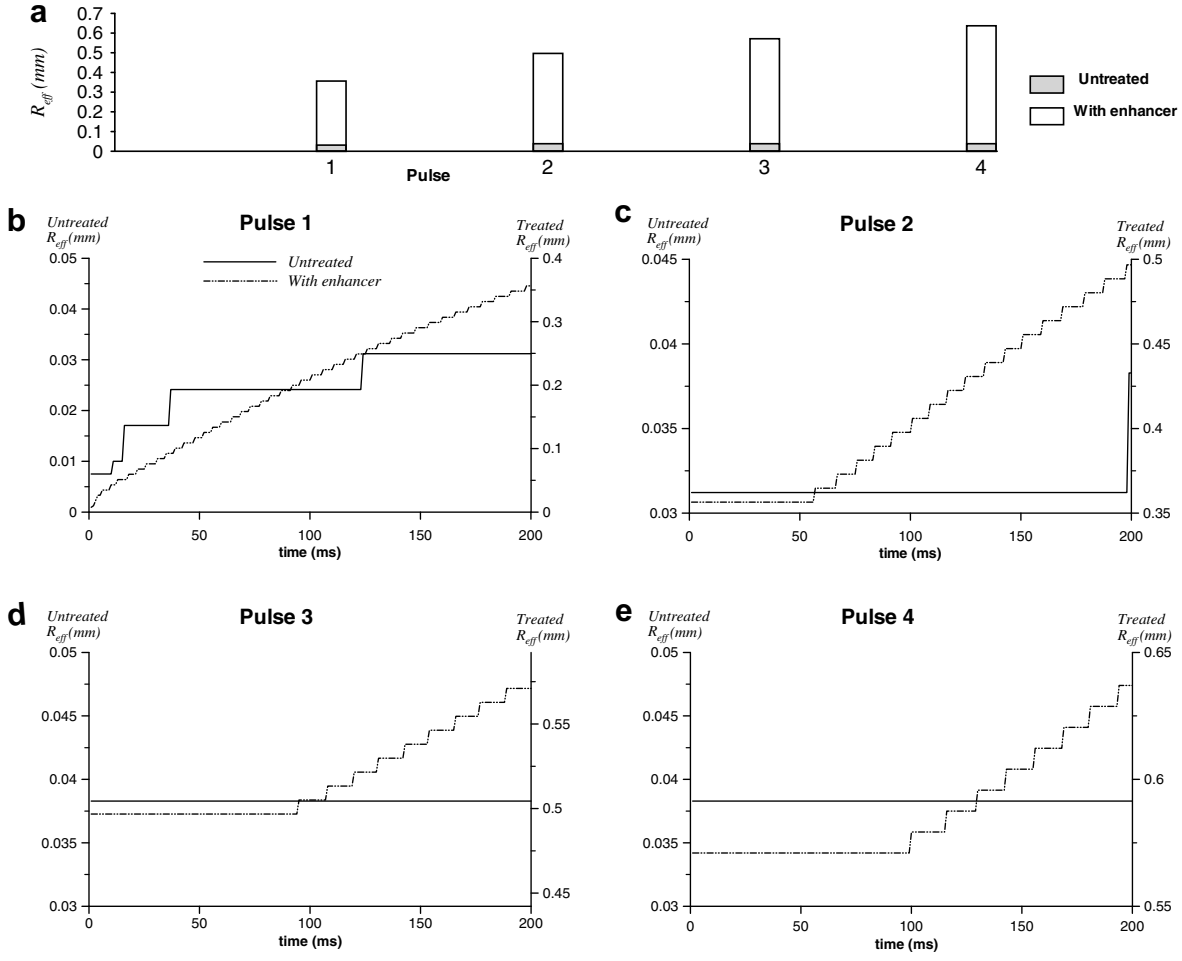

Fig. 7. Effective pore radius growth comparisons between treated and untreated skin exposed to 200 ms, 275 V pulses spaced at 1 s intervals. Effective pore radius is defined by the minimum radius at which lipids are unaffected by thermal phases change. In (b–e) effective pore radius for untreated skin shown on left axis, for skin treated with enhancer is shown on right axis.

occurring at locations farther away from the pre-existing pore. Furthermore at this time for the enhanced skin case, the radial location of highest apparent SC conductivity is nearly double that of the untreated skin. At the end of the first pulse ($t = 200$ ms) the potential solution of the untreated skin (Fig. 3b) shows remarkably little change from the earlier solution reflecting that little thermal disruption of the SC lipid structures has taken place. This is clearly not the case for the potential solution of the skin treated with the enhancer in Fig. 3d. The radius of the border at which the SC conductivity is unaltered is nearly ten times larger than the untreated case. With this change in SC electrical property, Fig. 3d shows a drastically reduced potential drop across the SC (especially in the region of lipid phase transition). Furthermore, the larger magnitude potential contours penetrate much lower into the tissue domain in the case with the enhancer. The electrical solutions reflect the thermal phase transition of the SC lipid structures, and specifically show that due to the lower transition temperatures, treating the skin results in a much larger radius in which the SC experiences electrical breakdown.

Transient thermal solutions of the 275 V pulse are shown at representative times for the normal skin in Fig. 4a–c and for skin treated with the enhancer in Fig. 4d–f. The small insets show a close-up of the SC in which the lipid melt fraction contours are depicted at low lipid melt fraction ($\varphi = 0.1$) and nearly fully fluidized lipid structures ($\varphi = 0.9$). Recalling the results of the electrical solution, it is expected that the small effective pore radius (at $t = 20$ ms) is associated in a large local current density which then results in large local Joule heating values and subsequent local temperature rises. This is confirmed for both treated and untreated skin in Fig. 4a and d in which local temperatures exceed 100 °C at the interface of the pre-existing pore and the epidermis. For the untreated skin over the course of the 200 ms pulse, the thermal profiles change little with the high temperature values exceeding 100 °C and remaining focused about the pre-existing pore (Fig. 4a–c). The insets show that for the untreated skin, the lipid structures change very little over the course of the 200 ms pulse and in fact at the end of the pulse, the lower level melt fraction contour reaching a radial distance less than 0.05 mm. This is not the case for the enhanced skin, which experiences the onset of lipid phase transition at a much lower value of 45 °C. The results of the lowered transition temperatures are reflected in the inserts of Fig. 4e and f which depict the effective pore radius extending beyond 0.3 mm. A result of a larger effective pore radius is a drop in current density and resulting Joule heating. This is

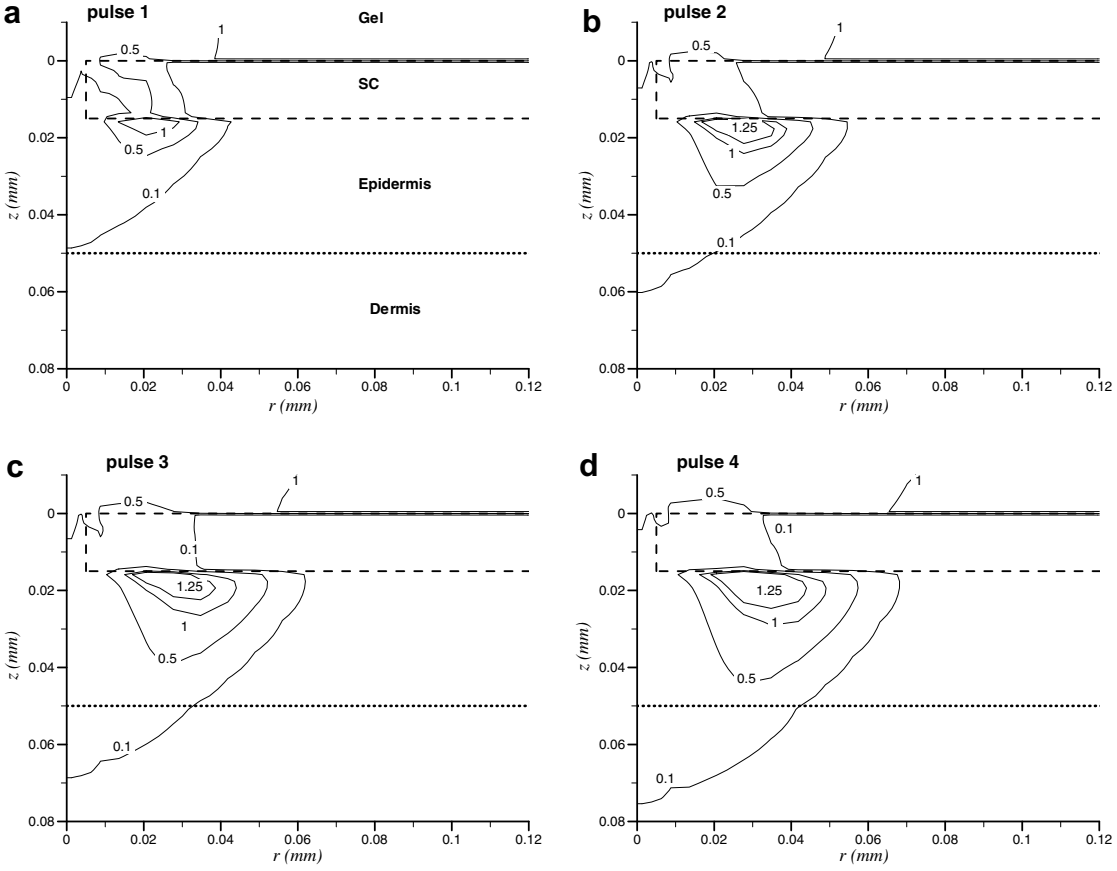

Fig. 8. Dimensionless concentration solution, C, of skin without enhancer treatment at the end of each of the four 275 V, 200 ms pulses applied at 1 s intervals. Dashed rectangle shows the boundary of the SC. Dotted lines represent interfaces between composite layers.

depicted in Fig. 4e at 100 ms, which shows the increase in the effective pore radius and resulting drop in the maximum temperature by about 50 °C. As the lower magnitude thermal contour levels propagate radially outward causing further lipid phase transitions and larger effective pore radius, the maximum temperature drops again to 75 °C in Fig. 4f.

Concentration solutions are discussed next. From the previous electrical and thermal solutions of untreated skin which show the highly concentrated profiles about the pre-existing pore, it is expected that the transport of solute concentration also remain in this vicinity. The concentration solution of solute transported through untreated skin is presented in Fig. 5. Initially only low concentration level contours penetrate the SC, clearly following the path through the pre-existing pore (Fig. 5a). After 100 ms pulsing (Fig. 5b), mid-level concentration level contours are seen penetrating through the SC. These seem to follow the large potential gradients within the SC and local regions of increased SC mobility values associated with the thermal phase transitions. A depletion of solute in the applicator gel is evident directly above this portion of the SC. At the end of the pulse (Fig. 5c) a local accumulation of solute is seen in the higher concentration located at the lower SC – epidermis interface. This may be explained by recalling that the electrophoretic term of Eq. (17) is a function of the gradient in potential. Within the SC the apparent electrical conductivity values are much lower than those of the epidermis below. This results in a larger potential gradient within the SC compared to the epidermis below. Effectively the electrophoretic driving forces carry the solute through the SC and then experience a sudden drop in magnitude. Due to the small effective pore radius associated with the untreated skin, even at the end of the 200 ms pulse, concentrations of solute are restricted to the center of the domain and are not transported past the epidermal–dermal junction.

Fig. 6a–d show the concentration profiles during a 200 ms, 275 V pulse for skin treated with the enhancer. Similar to the untreated case, at early pulsing times only low concentrations penetrate the skin through the pre-existing pore. At 60 ms pulsing, moderate concentrations have begun penetrating the SC. By 100 ms a deposition of solute is seen along the interface of the SC and epidermis. In fact the concentration at this location exceeds the initial concentration of the gel (Fig. 6c). This is attributed to the previously mentioned drop in electrophoretic forces as the solute moves from the SC into the epidermis. The lower temperature thermal behavior of the SC's barrier lip-

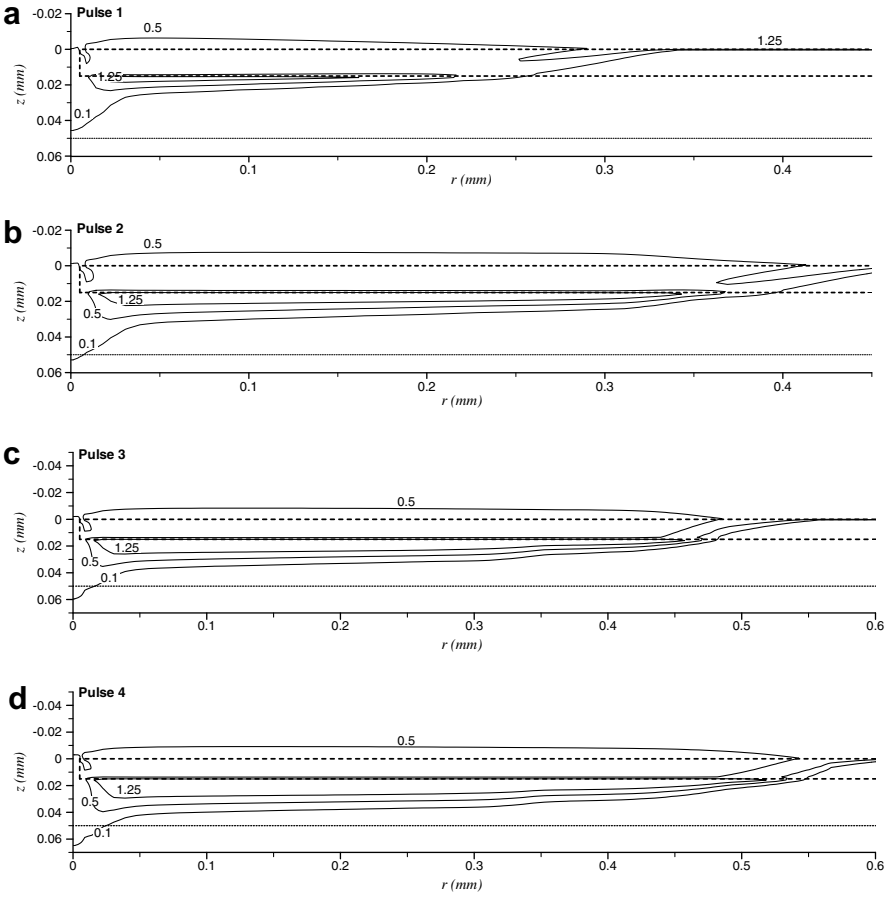

Fig. 9. Concentration solution, C, of skin treated with enhancer at the end of each of the four 275 V, 200 ms pulses applied at 1 s intervals. Dashed rectangle shows the boundary of the SC. Dotted lines represent interfaces between composite layers.

ids result in increased mobility at radial locations much greater than in the untreated skin. By the end of this pulse (Fig. 6d), the upper and mid-level concentration contours have reached 0.2 mm, a distance nearly ten times that of the untreated case. The concentration profiles of the treated skin are characterized by a shallow penetration distance coupled with a large radial distance.

4.2. Multiple pulses

Electroporation typically consists of multiple pulses spaced at regular intervals. In this study electroporation is modeled by four 275 V, 200 ms long DC pulses applied at 1 s intervals.

To compare the effects of the enhancer on transdermal delivery of solute, comparisons over the four pulse periods are made between skin treated with and without the enhancer.

Fig. 7 compares thermal pore formation of the normal to treated skin by showing the effective pore radius at the end of each pulse (Fig. 7a) as well as the growth of the pore during pulsing (Fig. 7b–e). The effective pore radius is defined by the minimum radius at which lipids are unaffected by thermal phases change. In both cases the first pulse produces the greatest pore growth followed by much slower rate of growth in later pulses, although the treated skin experiences remarkably larger pore sizes. After the first pulse, the untreated skin experiences negligible growth since the growth of the effective pore radius in the first pulse drops the local current density to such an extent that in subsequent pulses the Joule heating is not sufficient to cause temperature rises required to increase the effective pore by lipid melting. Even though the current density and subsequent Joule heating and temperature rises decrease with increased pore diameter, for the skin treated with the enhancer, the lower phase transition temperatures of the lipids are reached, thus allowing for continued pore growth in subsequent pulses.

The previous results of the single pulse case clearly show that without the enhancer, the solute is delivered to a small region just below the SC. This is also the case when multiple pulses are applied. Fig. 8 shows the concentration profiles at the end of each of the four pulses when the skin is untreated. As additional pulses are applied, the solute continues to accumulate at the lower SC epidermal border. The radial distance to which the solute penetrates into

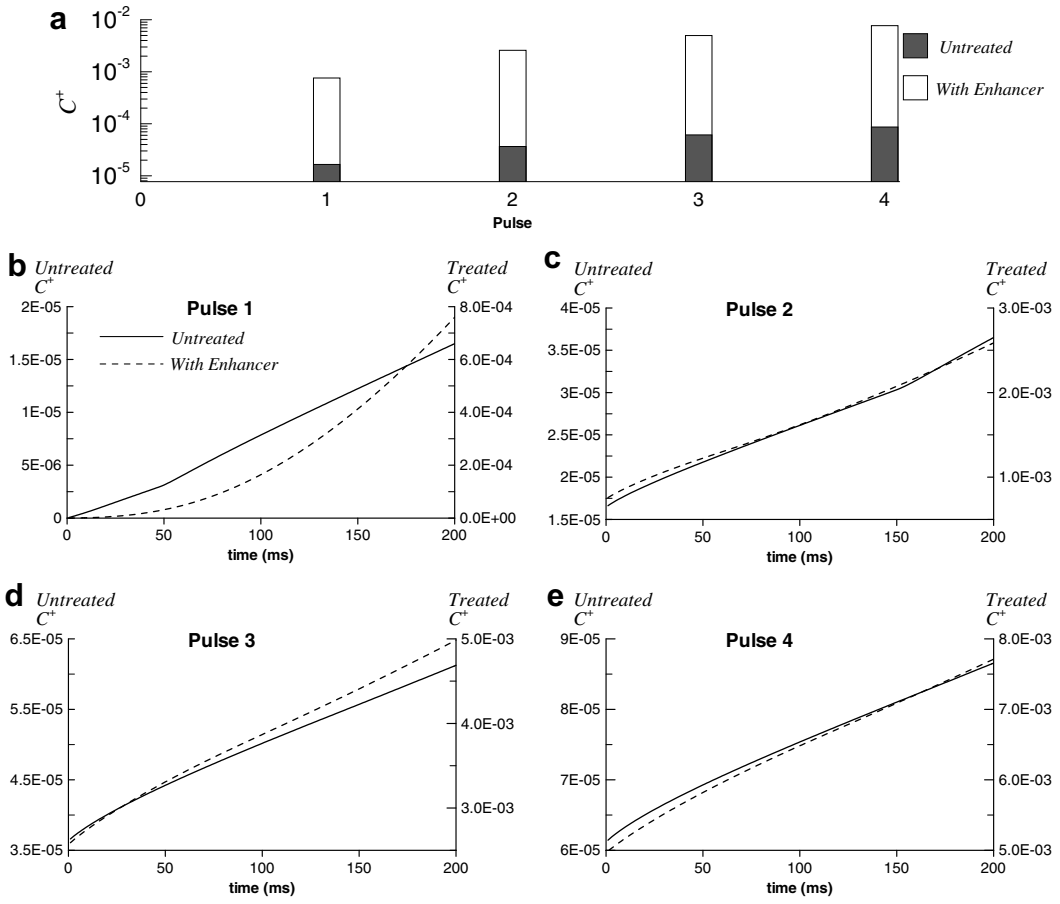

Fig. 10. Dimensionless relative concentration comparisons between treated and untreated skin exposed to 200 ms, 275 V pulses spaced at 1 s intervals. Dimensionless relative concentration delivered is defined by Eq. (31) and represents the ratio of solute delivered below the SC surface to that initially in the gel above the SC surface. In (b–e) concentration for untreated skin shown on left axis, for skin treated with enhancer is shown on right axis.

the SC does not increase with number of pulses administered. This is indicative of the limit of the thermal growth of the effective pore radius. An interesting artifact of this scenario is that as the electrophoretic forces continue to deliver solute through the small effective pore radius the solute concentrations wrap around the unperturbed SC as seen in the 0.1 concentration contour in Fig. 8d. As pulsing continues, lower level concentrations penetrate the upper epidermis.

The delivery of solute into the untreated skin behaves much differently. Fig. 9 depicts solute concentrations at the end of each pulse in treated skin. As expected from the previous results the lower lipid phase transition temperatures allow for a larger effective pore radius. In this case, as pulsing continues the solute penetrates the SC at increased radial distances, reflecting lipid melting by increased SC mobility. At the outer edge of the effective pore, the wrapping effect of the untreated skin case is not evident; in its place are contours that gradually slope toward the SC surface, indicating increased concentrations within the upper SC regions. The deposition of solute along the interface of the SC and epidermis continues to grow radially with pulsing. This region exceeds the initial concentration of the solute in the gel. It is interesting to note that the treated SC does not allow the solute to penetrate into the epidermis under the entire region of the effective pore, but only at locations near the axial center. This is a direct result of lower axial potential gradient that occurs as the SC becomes more electrically conductive by lipid melting.

In order to show the overall effects on transdermal delivery by using the chemical enhancer, a comparison is made representing the total solute delivered into the skin. To do this, the dimensionless relative concentration, C^+, is defined as

$$C^+(t) \equiv \frac{\int_0^{z\,\max} \int_0^{R_0} C(r,z,t)\mathrm{d}r\,\mathrm{d}z}{\int_{z\,\min}^{0} \int_0^{R_0} C(r,z,0)\mathrm{d}r\,\mathrm{d}z} \tag{31}$$

Essentially this parameter measures the ratio of solute transported below the surface of the SC to the total solute initially contained in the gel prior to the onset of the first electroporation pulse. The results of using the terpene enhance on total solute transport are shown in Fig. 10. Upon the onset of the first pulse, it is obvious that lowering the lipid transition temperatures results in an immediate increase in delivery. At the end of four pulse cycles, the treated skin shows an increase of solute delivery of nearly two orders of magnitude.

5. Conclusions

A transient three-dimensional model of in vivo skin electroporation incorporating SC lipid melting has been developed in which electrical and transient thermal solutions are found. Large molecule transdermal transport is modeled by the Nernst–Planck equation with low mobility values. A comparison study is conducted between skin treated with the enhancer terpene d-limonene that acts to lower the lipid thermal phase transition temperatures and normal skin not treated with the enhancer. The lower lipid phase transition temperatures associated with the treated skin allow a larger effective pore size for given pulse parameters. Near the beginning of the first electroporation pulse the localized Joule heating is focused near the pre-existing pore for both treated and untreated skin and local temperatures exceed 100 °C. By the end of the pulse the maximum temperatures of the untreated skin remain at these high temperatures, while the lipids of the treated skin have melted to such an extent that the reduced local current density and Joule heating cannot sustain these temperatures and the maximum temperature is reduced to 75 °C. Solute transport in the untreated skin is restricted to the center of the domain by the small effective pore radius. The lower temperature thermal behavior of the treated SC barrier lipids result in increased mobility, and consequently solute is transported through the SC at radial locations much greater than in the untreated skin. Transport solutions of both cases exhibit local accumulation of concentrations below the SC-epidermis interface which exceed concentration values initially contained within the applicator gel.

References

[1] K.C. Madison, Barrier function of the skin: "la raison d'Être" of the epidermis, J. Invest. Dermatol. 121 (2) (2003) 231–241.
[2] J.A. Bouwstra, P.L. Honeywell-Nguyen, G.S. Gooris, M. Ponec, Structure of the skin barrier and its modulation by vesticular formulations, Progr. Lipid Res. 42 (2003) 1–36.
[3] C. Lombry, N. Dujardin, V. Préat, Transdermal delivery of macromolecules using skin electroporation, Pharm. Res. 17 (1) (2000) 32–37.
[4] A.R. Denet, R. Vanbever, V. Préat, Skin electroporation for transdermal and topical delivery, Adv. Drug Deliver. Rev. 56 (5) (2004) 659–674.
[5] V. Regnier, N. De Morre, A. Jadoul, V. Préat, Mechanisms of a phosphorothioate oligonucleotide delivery by skin electroporation, Int. J. Pharm. 184 (2) (1999) 147–156.
[6] U.F. Pliquett, C. A Gusbeth, Perturbation of human skin due to application of high voltage, Bioelectrochemistry 51 (1) (2000) 41–51.
[7] M.R. Prausnitz, The effects of electric current applied to the skin: a review for transdermal drug delivery, Adv. Drug Deliv. Rev. 18 (3) (1996) 395–425.
[8] U. Pliquett, T.E. Zewert, T. Chen, R. Langer, J.C. Weaver, Imaging of fluorescent molecule and small ion transport through human stratum corneum during high voltage pulsing: localized transport regions are involved, Biophys. Chem. 58 (1–2) (1996) 185–204.
[9] M.R. Prausnitz, Do high voltage pulses cause changes in skin structure? J. Control. Release 40 (3) (1996) 321–326.
[10] U. Pliquett, R. Langer, J.C. Weaver, Changes in the passive electrical properties of human stratum corneum due to electroporation, Biochim. Biophys. Acta 1239 (2) (1995) 111–121.
[11] R. Vanbever, V. Preat, In vivo efficacy and safety of skin electroporation, Adv. Drug Deliv. Rev. 35 (1999) 77–88.
[12] R. Vanbever, G. Langers, S. Montmayeur, V. Preat, Transdermal delivery of fentanyl: rapid onset of analgesia using skin electroporation, J. Control. Release 50 (1–3) (1998) 225–235.
[13] G.M. Golden, D.B. Guzek, R.R. Harris, J.E. Mckie, R.O. Potts, Lipid thermotropic transitions in human stratum corneum, J. Invest. Dermatol. 86 (3) (1986) 255–259.

[14] G.M. Golden, D.B. Guzek, A.H. Kennedy, J.E. Mckie, R.O. Potts, Stratum corneum lipid phase transition and water barrier properties, Biochemistry 26 (8) (1987) 2382–2388.
[15] H. Tanojo, J.A. Bouwstra, H.E. Junginger, H.E. Bodde, Thermal analysis studies on human skin and skin barrier modulation by fatty acids and propylene glycol, J. Therm. Anal. Calorim 57 (1999) 313–322.
[16] P.A. Cornwell, B.W. Barry, J.A. Bouwstra, G.S. Gooris, Modes of action of terpene penetration enhancers in human skin; differential scanning calorimetry, small angle diffraction and enhancer uptake studies, Int. J. Pharm. 127 (1996) 9–26.
[17] S.M. Al-Saidan, B.W. Barry, A.C. Williams, Differential scanning calorimetry of human and animal stratum corneum membranes, Int. J. Pharm. 168 (1998) 17–22.
[18] R.O. Potts, M.L. Francoeur, Lipid biophysics of water loss through the skin, Proc. Natl. Acad. Sci. USA 87 (10) (1990) 3871–3873.
[19] U.F. Pliquett, R. Vanbever, V. Preat, J.C. Weaver, Local transport regions (LTRs) in human stratum corneum due to long and short 'high voltage' pulses, Bioelectroch. Bioener. 47 (1998) 151–161.
[20] R. Vanbever, U.F. Pliquett, V. Preat, J.C. Weaver, Comparison of the effects of short, high-voltage and long, medium-voltage pulses on skin electrical and transport properties, J. Control. Release 60 (1999) 35–47.
[21] U. Pliquett, S. Gallo, S.W. Hui, C. Gusbeth, E. Neumann, Local and transient changes in stratum corneum at high electric fields: contribution of Joule heating, Bioelectrochemistry 67 (1) (2005) 37–46.
[22] S.A. Gallo, A. Sen, M.L. Hensen, S.W. Hui, Temperature-dependent electrical and ultrastructural characterization of porcine skin upon electroporation, Biophys. J. 82 (2002) 109–119.
[23] A.C. Williams, B.W. Barry, Penetration enhancers, Adv. Drug Deliv. Rev. 56 (5) (2004) 603–618.
[24] O. Pillai, R. Panchagnula, Transdermal iontophoresis of insulin – V. Effect of terpenes, J. Control. Release 88 (2) (2003) 287–296.
[25] J.L. Harden, J.-L. Viovy, Numerical studies of pulsed iontophoresis through model membranes, J. Control. Release 38 (2–3) (1996) 129–139.
[26] T.R. Mollee, Y.G. Anissimov, M.R. Roberts, Periodic electric field enhanced transport through membranes, J. Membr. Sci. 278 (1–2) (2006) 290–300.
[27] H.G. Zhu, K.D. Peck, S.K. Li, A.H. Ghanem, W.I. Higuchi, Quantifications of pore induction in human epidermal membrane during iontophoresis: the importance of background electrolyte solution, J. Pharm. Sci. 90 (7) (2001) 932–942.
[28] S.K. Li, A.H. Ghanem, C.L. Teng, G.E. Hardee, W.I. Higuchi, Iontophoretic transport of oligonucleotides across human epidermal membrane: a study of the Nernst–Planck model, J. Pharm. Sci. 90 (7) (2001) 915–931.
[29] G.T. Martin, U.F. Pliquett, J.C. Weaver, Theoretical analysis of localized heating in human skin subjected to high voltage pulses, Bioelectrochemistry 57 (2002) 55–64.
[30] P.F. Millington, R. Wilkinson, Skin, Cambridge University Press, Cambridge, Great Britain, 1983.
[31] F.M. Hendriks, D. Brokken, C.W.J. Oomens, F.P.T. Baaijens, Influence of hydration and experimental length scale on the mechanical response of human skin in vivo, using optical coherence tomography, Skin Research and Technology 10 (2004) 231–241.
[32] H.H. Pennes, Analysis of tissue and arterial blood temperatures in the resting forearm, J. Appl. Physiol. 1 (1948) 93–122.
[33] F.A. Duck, Physical Properties of Tissue: A Comprehensive Reference Book, Academic Press, London, 1990.
[34] L.O. Svaasand, L.L. Randeberg, G. Aguilar, B. Majaron, S. Kimel, E.J. Lavernia, J.S. Nelson, Cooling Efficiency of cryogen spray during laser therapy of skin, Lasers Surg. Med. 32 (2) (2003) 137–142.
[35] J.C. Chato, R.C. Lee, The future of biothermal engineering, Ann. NY Acad. Sci. 858 (1998) 1–20.
[36] S.B. Wilson, V.A. Spence, A tissue heat transfer model for relating dynamic skin temperature changes to physiological parameters, Phys. Med. Biol. 33 (8) (1988) 895–912.
[37] P. Wainwright, Thermal effects of radiation from cellular telephones, Phys. Med. Biol. 45 (8) (2000) 2363–2372.
[38] Y.A. Chizmadzhev, A.V. Indenbom, P.I. Kuzmin, S.V. Galichenko, J.C. Weaver, R.O. Potts, Electrical properties of skin at moderate voltages: contribution of appendageal macropores, Biophys. J. 74 (2) (1998) 843–856.
[39] D.A. Zaharoff, R.C. Barr, C.-Y. Li, F. Yuan, Electromobility of plasmid DNA in tumor tissues during electric field-mediated gene delivery, Gene Therapy 9 (19) (2002) 1286–1290.
[40] M.F. Bureau, J. Gehl, V. Deleuze, L.M. Mir, D. Scherman, Importance of association between permeabilization and electrophoretic forces for intramuscular DNA electrotransfer, Biochim. Biophys. Acta: General Subjects 1474 (3) (2000) 353–359.
[41] S. Satkauskas, F. Andre, M.F. Bureau, D. Scherman, D. Miklavcic, L.M. Mir, Electrophoretic component of electrical pulses determines the efficacy of in vivo DNA electrotransfer, Human Gene Therapy 16 (10) (2005) 1194–1201.
[42] M. Planck, Über die erregung von elektrizität und wärme in elektrolyten, Ann. Phys. Chem. 39 (1890) 161–186.
[43] P.A. Netti, D.A. Berk, M.A. Swartz, A.J. Grodzinsky, R.K. Jain, Role of extracellular matrix assembly in interstital transport in solid tumors, Cancer Res. 60 (2000) 2497–2503.
[44] D.A. Zaharoff, F. Yuan, Effects of pulse strength and pulse duration on in vitro DNA electromobility, Bioelectrochemistry 62 (1) (2004) 37–45.
[45] N.C. Stellwagen, DNA mobility anomalies are determined primarily by polyacrylamide gel concentration, not gel pore size, Electrophoresis 18 (1997) 34–44.
[46] C.L. Silva, S.C.C. Nunes, M.E.S. Eusebio, J.J.S. Sousa, A.A.C.C. Pais, Study of human stratum corneum and extracted lipids by thermomicroscopy and DSC, Chem. Phys. Lipids 140 (1–2) (2006) 36–47.
[47] C.L. Silva, S.C.C. Nunes, M.E.S. Eusebio, A.A.C.C. Pais, J.J.S. Sousa, Thermal behaviour of human stratum corneum – a differential scanning calorimetry study at high scanning rates, Skin Pharmacol. Physiol. 19 (3) (2006) 132–139.
[48] S.H. White, D. Mirejovsky, G.I. King, Structure of lamellar lipid domains and corneocyte envelopes of murine stratum corneum – an X-ray-diffraction study, Biochemistry 27 (10) (1988) 3725–3732.
[49] V.R. Voller, A.D. Brent, The modeling of heat, mass and solute transport in solidification systems, Int. J. Heat Mass Transfer 32 (9) (1989) 1719–1732.
[50] M.N. Ozisik, Heat Conduction, John Wiley & Sons, New York, NY, USA, 1993.
[51] G.C.J. Bart, P.C. Van der Laag, Modeling of arbitrary-shaped specific and latent heat curves in phase-change storage simulation routines, Trans. ASME J. Solar Energy Eng. 112 (1990) 29–33.
[52] S.K. Roy, B.L. Avanic, Turbulent heat transfer with phase change material suspensions, Int. J. Heat Mass Transfer 44 (12) (2001) 2277–2285.
[53] W.H.M. Craane van Hinsberg, J.C. Verhoef, H.E. Junginger, H.E. Bodde, Thermoelectrical analysis of the human skin barrier, Thermochim. Acta. 248 (1995) 303–318.
[54] N. Dujardin, E. Staes, Y. Kalia, P. Clarys, R. Guy, V. Preat, In vivo assessment of skin electroporation using square wave pulses, J. Control. Release 79 (1–3) (2002) 219–227.
[55] U. Pliquett, C. Gusbeth, Surface area involved in transdermal transport of charged species due to skin electroporation, Bioelectrochemistry 65 (1) (2004) 27–32.
[56] S.V. Patankar, Numerical Heat Transfer and Fluid Flow, Hemisphere, Washington DC, 1980.